On the terminal velocity of single bubbles rising in non-Newtonian power-law liquids

Journal of Non-Newtonian Fluid Mechanics 278 (2020) 104249

Contents lists available at ScienceDirect

Journal of Non-Newtonian Fluid Mechanics

journal homepage: www.elsevier.com/locate/jnnfm

On the terminal velocity of single bubbles rising in non-Newtonian power-law liquids

A. Battistella [a], S.J.G. van Schijndel [a], M.W. Baltussen [b], I. Roghair [a,*], M. van Sint Annaland [a]

[a] Chemical Process Intensification, Department of Chemical Engineering and Chemistry, Eindhoven University of Technology, Eindhoven, the Netherlands
[b] Multi-scale Modeling of Multiphase Flows, Department of Chemical Engineering and Chemistry, Eindhoven University of Technology, Eindhoven, the Netherlands

ARTICLE INFO

Keywords:
Front-tracking
Bubbly flows
Drag force
Non-Newtonian fluids
Direct Numerical Simulations

ABSTRACT

To describe bubbly flows, an accurate prediction of the bubble rise velocity is crucial. For non-Newtonian fluids, closures for the bubble rise velocity provided in the literature are usually empirical and rather restricted in their applicability. In this work, a Front-Tracking Computational Fluid Dynamics model has been used to investigate the behaviour of a single bubble rising in a power-law fluid, for a very wide range of viscosities covering both shear-thinning and shear-thickening behaviour, where the power-law exponent n was varied between 0.5 and 1.5 and for three different bubble diameters (viz. 0.5 mm, 2 mm and 4 mm). The non-Newtonian behaviour of the continuous phase strongly influences the shape of the single rising bubbles caused by the viscosity profiles that develop in the flow field. As a consequence, large non-spherical bubbles become more spherical in shear-thickening fluids (in comparison to the same bubble in a Newtonian liquid), whereas small spherical bubbles lose their sphericity in shear-thinning fluids. To determine the bubble rise velocity for bubbles in non-Newtonian fluids with a power law behaviour, the drag closure derived for bubbles rising in Newtonian liquids proposed by Dijkhuizen et al. (2010), which combines viscous drag and shape-induced drag in a single correlation, is adapted using a modified Reynolds number. In this work it is shown that this adapted correlation is able to predict the terminal rise velocity of single bubbles rising in non-Newtonian power-law fluids within 20% accuracy for the majority of the investigated cases, provided that the drag regime does not change.

1. Introduction

Bubbly flows are encountered in a multitude of unit operations in a large variety of industrial applications. Often, the continuous liquid phase exhibits non-Newtonian behaviour, as e.g. in bioreactors [2] or in polymers production (e.g. polycondensation or polymer devolatilization) [3].

For the design and optimization of process equipment involving bubbly flows it is crucial to accurately predict the bubble rise velocity, since this will largely determine the column hydrodynamics and mass/heat transfer characteristics, and consequently the performance of the equipment. In the pseudo steady-state, the balance between the drag force and the buoyancy forces determines the terminal rise velocity. Although non-Newtonian fluids are common in industry, a complete description of the drag coefficient for a bubble rising in such fluids is still not available [4]. In most cases, the provided closures are empirical and usually limited in their applicability.

With the increase in computational power, numerical simulation has proven to be an effective tool in gaining fundamental understanding of multi-phase gas-liquid flows. In the framework of Computational Fluid Dynamics (CFD), a multi-scale modelling strategy has been applied [5–7], where micro-scale detailed models are used to develop closure relations for unresolved, higher scale models, such as Euler–Lagrange and Euler–Euler models (see Fig. 1). The latter treats both phases as a continuum, basically averaging bubble properties on the Eulerian grid, while the former includes more details by tracking each bubble in a Lagrangian manner. Despite the loss of details compared to lower scale models, these methods are computationally favorable, allowing simulations up to industrial scale. On the other hand, the accuracy of the applied closures, for instance to describe phase interactions (hydrodynamic forces, mass and heat transfer), strongly influences the quality of the simulation results of these unresolved models.

Direct Numerical Simulations (DNS) represents a viable option to study phase interactions, to gain fundamental understanding of the physics of bubbly flows and to obtain closures for higher scale models. This approach has been demonstrated in the past for Newtonian fluids [1,8,9], where it has been applied for the study of the drag and lift forces on single bubbles and bubbles rising in swarms.

Previously, bubbles in non-Newtonian fluids have been studied using different CFD models. Wu [10] used *Fluent 12.0* to perform Euler-Euler

* Corresponding author.
E-mail address: I.Roghair@tue.nl (I. Roghair).

https://doi.org/10.1016/j.jnnfm.2020.104249
Received 23 September 2019; Received in revised form 9 January 2020; Accepted 12 February 2020
Available online 19 February 2020

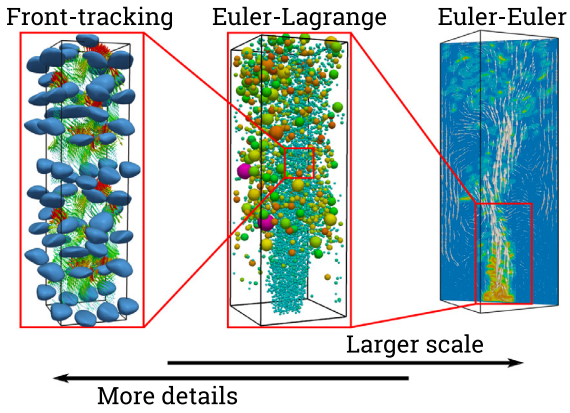

Fig. 1. Multi-scale modelling strategy for bubbly flows, depicting a Front-Tracking model (Direct Numerical Simulations), a Discrete Bubble Model (Euler–Lagrange) and a Two-Fluid model (Euler–Euler) (adapted from Lau et al. [7]).

simulations of bubbles rising in shear-thinning fluids in anaerobic digesters, although using a drag law derived for Newtonian fluids. Lattice Boltzmann methods have been successfully employed in the past for simulations of bubbles rising in complex fluids. For instance, Frank and Li [11] simulated a sixth-order Maxwell fluid and were able to capture the negative wake and the bubble teardrop shape, which corresponded to their experimental data. In addition, Liu et al. [12] employed a Volume of Fluid (VOF) method to study the behavior of multiple bubbles (couples and triplets) rising in shear-thinning fluids. This study focused mostly on collisions and coalescence. Radl et al. [13] investigated the rise of bubbles in different viscous and viscoelastic fluids, with the inclusion of mass transfer, with a hybrid 2D Front-Tracking/Front-Capturing model. Their simulations were limited to 2D, due to the high grid resolution needed by the species solver. Zhang et al. [14] adopted a level-set method to investigate the velocity and viscosity distribution around a single bubble rising in a shear-thinning fluid, described by a Carreau viscosity model. Some attempts have been done in the past to adapt existing drag correlations to non-Newtonian power-law fluids, such as Rodrigue [15], who considered shear-thinning polymers at low to moderate Reynolds numbers. The proposed correlation is not suitable for high Reynolds numbers, where it does not converge to a constant as has been well-established in recent years. More recently, Ohta et al. [16, 17] developed a Coupled Level Set Volume of Fluid model, which they used to study the shape and velocity of bubbles rising in both shear-thinning and shear-thickening power-law fluids, and compared it with experimental data. Premlata et al. [18, 19] also used a VOF method with adaptive grid refinement to study the behaviour of bubbles rising in Carreau–Yasuda fluids. Their study focused on the three-dimensional rising behaviour of single bubbles, and they were able to qualitatively compare their experimentally obtained images of the bubbles to simulation results. The same model has been applied to study viscosity-stratified fluids and viscoplastic materials [20–22]. An extensive analysis of bubbles rising in viscoplastic fluids has been provided by Tsamopoulos et al. [23], where the bubble rise velocity and the drag coefficient are determined assuming axial symmetry and steady flow. Perhaps the most relevant work related to this manuscript is the one of Chhabra [24], where it has been found that standard Newtonian correlations can be adapted to well predict the drag coefficient of non-deformable, solid spheres in shear-thinning power-law fluids, as demonstrated by experimental results.

A comprehensive quantitative description of the drag coefficient for bubbles rising in non-Newtonian fluids has not yet been reported in literature, to the knowledge of the authors. The aim of this work is thus to fill this gap and give a description of the drag coefficient for power-law non-Newtonian fluids (both shear-thickening and shear-thinning), following the approach of Dijkhuizen et al. [1] and starting from single bubbles. The starting hypothesis is that it is possible to correct an existing correlation for Newtonian fluids, as for instance the one of Dijkhuizen et al. [1], to account for the non-Newtonian behavior of the liquid using a generalized Reynolds number [24], as will be explained later.

The manuscript is organized as follows: first, the Front-Tracking model used in this work is described and verified. Subsequently, the bubble shapes and viscosity profiles for non-Newtonian fluids will be investigated. To conclude, an outline of the drag coefficient for different power-law fluids will be proposed.

2. Model description

The Front-Tracking model used in this work has previously been developed, validated and applied for simulations of bubbles rising in Newtonian liquids. An extensive description of the model and its extensive validation for bubbles rising in a liquid can be found in Dijkhuizen et al. [1], Baltussen et al. [25, 26] and Roghair et al. [27, 28]. In this paper, the model will only be shortly introduced with particular focus on the implementation of the non-Newtonian viscosity model. For further details the reader is referred to the aforementioned papers.

2.1. Hydrodynamics modeling

In the Front Tracking model the surface of the bubbles is represented by a triangulated mesh, where the fluid flow (both in the dispersed and continuous phase) is described by the incompressible Navier–Stokes equations and continuity equation using a one-field approximation:

$$\rho\frac{\partial \mathbf{u}}{\partial t} + \rho\nabla\cdot(\mathbf{uu}) = -\nabla p + \rho\mathbf{g} + \nabla\cdot\boldsymbol{\tau} + \mathbf{F}_\sigma \tag{1a}$$

$$\nabla\cdot\mathbf{u} = 0 \tag{1b}$$

where $\mathbf{u}$ is the fluid velocity, $\boldsymbol{\tau}$ is the stress tensor, which will be described in more detail in the next sections, and $\mathbf{F}_\sigma$ represents a singular source-term for the surface tension force at the interface:

$$\mathbf{F}_{\sigma,i\to m} = \sigma\left(\mathbf{t}_{mi}\times\mathbf{n}_{mi}\right) \tag{2}$$

which is calculated from the position and orientation of the interfacial markers [28]. The equations are discretized with a finite-difference technique on a staggered Eulerian grid. The convection terms and the off-diagonal terms of the stress tensor are discretized explicitly, while the diagonal terms of the stress tensor are discretized implicitly resulting in a semi-implicit treatment of the stress tensor enhancing the numerical stability. The flow field is solved using a two-stage projection-correction method, where a pressure-correction step based on the continuity equation is taken iteratively after solving the three dimensional momentum balance equations. Both the implicit part of the stress tensor and the pressure correction are solved with an incomplete Cholesky conjugate gradient (ICCG) method [8,29]. To approximate an infinite quiescent liquid medium, a free-slip boundary condition is applied at the domain walls. The window shifting technique [5] is used to keep the bubble at approximately the same position relative to the domain, which reduces the computational costs.

2.2. Surface mesh

The gas-liquid interface is composed of Lagrangian tracking points, connected to form a triangular mesh, where each of the triangular cells is called a surface marker. The Lagrangian points are moved with the local liquid velocity, which is interpolated from the fluid velocity field to the Lagrangian tracking points using cubic splines, using a 4th order Runge–Kutta time stepping scheme. As a consequence of the separate movement of each marker point, the triangular markers change their configuration at every time step, which will eventually lead to a decrease in the mesh quality and therefore a decrease in the overall accuracy of the surface

tension force calculation. Moreover, the bubble volume may no longer be conserved. To maintain good interface mesh quality, ensure bubble volume conservation and enhance model performance, (volume conservative) remeshing is an important step in the Front-Tracking technique. A detailed description of the applied remeshing procedures can be found in Roghair et al. [27, 28].

2.3. Viscosity model

In (inelastic) non-Newtonian fluids, the apparent shear viscosity is not constant, as in Newtonian fluids, but is a function of the shear rate. For a Newtonian fluid, the stress tensor $\boldsymbol{\tau}$ is given by:

$$\boldsymbol{\tau} = -\mu\left(\nabla\mathbf{u} + (\nabla\mathbf{u})^T\right) \equiv -\mu\dot{\boldsymbol{\gamma}} \tag{3}$$

in which $\dot{\boldsymbol{\gamma}}$ represents the rate of strain tensor. A frequently applied model to describe the rheology of non-Newtonian fluids, excluding visco-elastic behaviour, is the *generalized Newtonian model*, which simply replaces the viscosity μ in Eq. (3) with an apparent viscosity η as a function of the shear rate [30]. The shear rate can be written as the magnitude of the rate of strain tensor:

$$\dot{\gamma} = \sqrt{\frac{1}{2}(\dot{\boldsymbol{\gamma}} : \dot{\boldsymbol{\gamma}})} \tag{4}$$

With the generalized Newtonian model, the stress tensor is calculated as:

$$\boldsymbol{\tau} = -\eta\left(\nabla\mathbf{u} + (\nabla\mathbf{u})^T\right) \equiv -\eta\dot{\boldsymbol{\gamma}}$$

$$\text{with} \quad \eta = \eta(\dot{\gamma}) \tag{5}$$

Several empirical models have been proposed in the literature to describe the relation between η and the shear rate, and the simplest and most widely used correlation is the power-law model (or Ostwald – de Waele relationship):

$$\eta = K\dot{\gamma}^{n-1} \tag{6}$$

In Eq. (6), K represents the consistency index, while n is the flow behaviour index, a constant characterizing the fluid: for $n = 1$ the relation reduces to a Newtonian fluid, for $n < 1$ the fluid is shear-thinning (viscosity reduces with the shear rate) and for $n > 1$ the fluid is shear-thickening (viscosity increases with the shear rate). Although often applied, this model contains a very important physical and numerical shortcoming, as discussed by Gabbanelli et al. [31]. When the fluid is quiescent, or in general in a zero-shear situation, the viscosity becomes infinite for a shear-thinning rheology, while it becomes zero for shear-thickening fluids. Moreover, most non-Newtonian fluids present even more complex behaviour than what is captured with a power-law expression: for instance, they often show Newtonian plateaus around a limited non-Newtonian region. More complex models have been developed to overcome this problem, such as the Carreau model, but these models are usually only valid for a limited type of behaviour (e.g. shear-thinning). A simple but effective solution is to use a *truncated power-law* model [31]:

$$\eta = \eta(\dot{\gamma}) = \begin{cases} \eta_0, & \dot{\gamma} < \dot{\gamma}_0 \\ K\dot{\gamma}^{n-1}, & \dot{\gamma}_0 \le \dot{\gamma} \le \dot{\gamma}_\infty \\ \eta_\infty, & \dot{\gamma} > \dot{\gamma}_\infty \end{cases} \tag{7}$$

where η_0 and η_∞ are the viscosities calculated with the respective limiting shear rates. To keep consistency between the different cases, it has been chosen to express the limits in terms of η, as described in Table 1. Note that the + or − subscripts in Table 1 represent 0 or ∞, according to the rheology of the selected fluid, *i.e.* for shear-thinning liquids + and − represent 0 and ∞, respectively, while for shear-thickening liquids + and − represent ∞ and 0. Although these limits guarantee numerical stability especially during the first time step, when the fluid is quiescent and there is no shear, the limits are selected wide enough to maintain a power-law rheology in the whole domain for the remaining of the simulations and thus the selected limits do not affect the terminal rise velocity of the bubbles.

Table 1
Truncation limits for the power-law model for each consistency index K.

K[Pas^n]	η_-[Pas]	η_+[Pas]
10^{-3}	10^{-5}	10^{19}
10^{-2}	10^{-4}	10^{20}
10^{-1}	10^{-3}	10^{21}

2.4. Physical properties

Since the interface position is exactly known, the phase fraction ϕ in each Eulerian cell can be computed exactly through geometrical analysis [29]. If a cell contains both liquid and gas, the physical properties density and viscosity need to be scaled accordingly into a macroscopic property. The density of the fluid cell is calculated by weighted averaging with the phase fraction, while the viscosity (or the non-Newtonian apparent viscosity) is calculated via harmonic averaging of the kinematic viscosities following the work of Prosperetti [32]:

$$\rho(\mathbf{x}) = \sum_{p=0}^{n_{\text{phase}}-1} \phi_p(\mathbf{x})\rho_p \tag{8a}$$

$$\frac{\rho(\mathbf{x})}{\mu(\mathbf{x})} = \sum_{p=0}^{n_{\text{phase}}-1} \phi_p(\mathbf{x})\frac{\rho_p}{\mu_p} \tag{8b}$$

2.5. Drag coefficient

In previous works, the Front-Tracking model has been used to derive a drag correlation for both single bubble [1] and bubbles rising in a swarm [8]. The terminal velocity of a bubble is determined by a force balance between buoyancy and drag, as described by Roghair et al. [8]. Assuming that the liquid is infinite with zero bulk velocity, the drag coefficient can be expressed as:

$$C_D = \frac{4}{3}\frac{d_b\left(\rho_l - \rho_g\right)\mathbf{g}}{\rho_l\left|\mathbf{u}_\infty\right|^2} \tag{9}$$

The aim of this paper is to give a comprehensive description of the drag coefficient of single bubbles rising in non-Newtonian power-law fluids. Thus, the starting point is the adoption of the drag correlation obtained by Dijkhuizen et al. [1]. In particular, Dijkhuizen et al. [1] described the drag coefficient as:

$$C_D = \sqrt{C_D(\text{Re})^2 + C_D(\text{Eo})^2} \tag{10}$$

where the Reynolds dependent part, as described by a correlation developed by Mei et al. [33], is used to model the frictional stress (for smaller spherical bubbles):

$$C_D(\text{Re}) = \frac{16}{\text{Re}}\left(1 + \frac{2}{1 + \frac{16}{\text{Re}} + \frac{3.315}{\text{Re}}}\right) \tag{11}$$

and the Eötvös dependent part, fitted by Dijkhuizen et al. [1], is used to model the form-drag (i.e. shape-induced, for large deformable bubbles):

$$C_D(\text{Eo}) = \frac{4\text{Eo}}{9.5 + \text{Eo}} \tag{12}$$

This correlation achieves a smooth transition when shifting from spherical to deformed bubbles [1].

The Eötvös number can be easily calculated a priori, using physical properties and the bubble diameter:

$$\text{Eo} = \frac{g\Delta\rho d_b^2}{\sigma} \tag{13}$$

However, the Reynolds number in Eq. (11)) depends amongst other parameters on the fluid viscosity (which depends on the local shear rate)

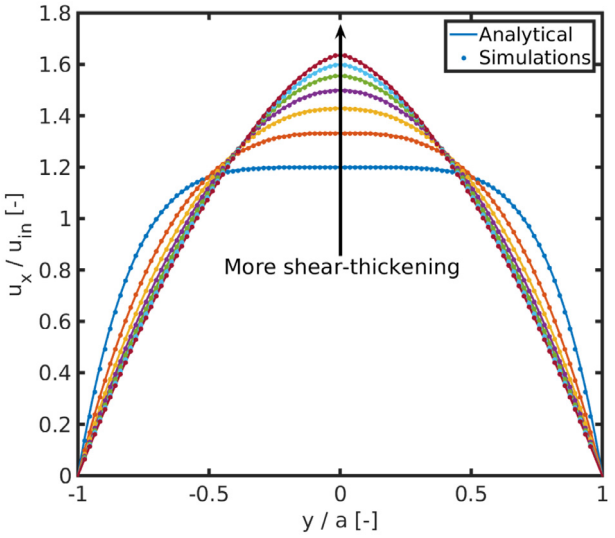

Fig. 2. Comparison of simulation results with their analytical solutions for the steady-state velocity profile of a 2D single phase non-Newtonian flow between two parallel plates for different power-law exponents (following the direction of the arrow: $n = 0.2; 0.5; 0.8; 1; 1.2; 1.5; 1.8$).

Table 2
Relative error between the numerical and analytical solutions of the velocity profile for a 2D single phase non-Newtonian flow between two parallel plates.

n	ϵ_{rel}
0.2	0.36%
0.5	0.13%
0.8	0.11%
1	0.10%
1.2	0.10%
1.5	0.10%
1.8	0.10%

and the bubble rise velocity. The latter is obtained from the simulation as the time-averaged rate of displacement of the bubble center of mass. The viscosity, in contrast, cannot be directly taken from the simulation results, as it is represented by a field, not by a single, well-defined value as in Newtonian fluids. Instead, the definition for the generalized Reynolds number for power-law fluids, as introduced by Chhabra [34], is used in this work:

$$\mathrm{Re}^* = \frac{\rho u^{2-n} d_b^n}{K} \tag{14}$$

The rationale behind this choice is that the physics determining the drag coefficient is not altered by the fluid rheology (as for instance with contaminated fluids) but can rather be captured by the changing apparent viscosity in a similar way as for Newtonian liquids, thus using the modified Reynolds number given in Eq. (14). This has been demonstrated for spheres in shear-thinning liquids by Chhabra [24].

3. Verification

The used Front-Tracking model has been thoroughly validated before by Dijkhuizen et al. [1] and Roghair et al. [8] for a wide range of Newtonian liquids and bubble sizes. In this paper the model verification focuses on the implementation of the non-Newtonian truncated power-law viscosity model and on the grid convergence study.

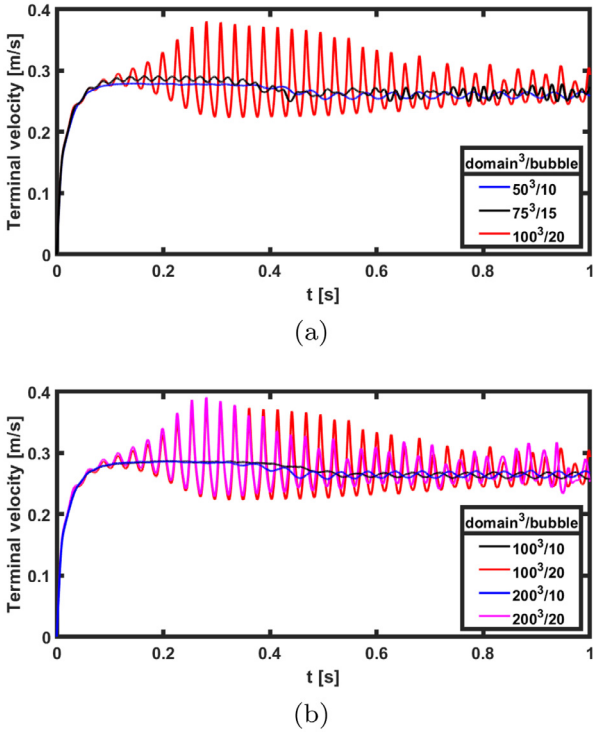

Fig. 3. Rising velocity of a 4 mm bubble rising in a shear-thinning $n = 0.5$ fluid. (a) Constant bubble to domain ratio (1:5) and (b) varying domain and bubble size.

Table 3
Terminal velocity for a 4 mm bubble at different grid resolutions.

n	d_b	domain^3	$u_{t,simulated}$ [ms^{-1}]
0.5	10	50	0.2647
	10	100	0.2709
	20	100	0.2744
	20	200	0.2757
1	10	50	0.2743
	10	100	0.2770
	20	100	0.2784
	20	200	0.2818
1.5	10	50	0.2405
	10	100	0.2456
	20	100	0.2460
	20	200	0.2509

3.1. Viscosity model

To verify the correct implementation of the viscosity model, a simple test case is represented by a single phase unidirectional pressure-driven flow between two parallel plates, separated by a distance $2L$ in the y direction, orthogonal to the flow direction x. Assuming that the only non-zero velocity component is $u_x(y)$, it is possible to simplify the Navier-Stokes equations (see Eqs. (1a) and (1b)) to obtain the stationary velocity profile as:

$$\begin{aligned} u_x(y) &= L\frac{n}{n+1}\left(\frac{L}{K}\frac{\partial p}{\partial x}\right)^{1/n}\left(1-\left|\frac{y}{L}\right|^{\frac{n+1}{n}}\right) \\ &= u_{in}\frac{2n+1}{n+1}\left(1-\left|\frac{y}{L}\right|^{\frac{n+1}{n}}\right) \end{aligned} \tag{15}$$

where u_{in} represents the inlet velocity, and y the distance from the center of the channel in the positive or negative direction, as it is symmetric. For a liquid described with the truncated power-law viscosity model (Eq. (7)) three distinct regions can be identified:

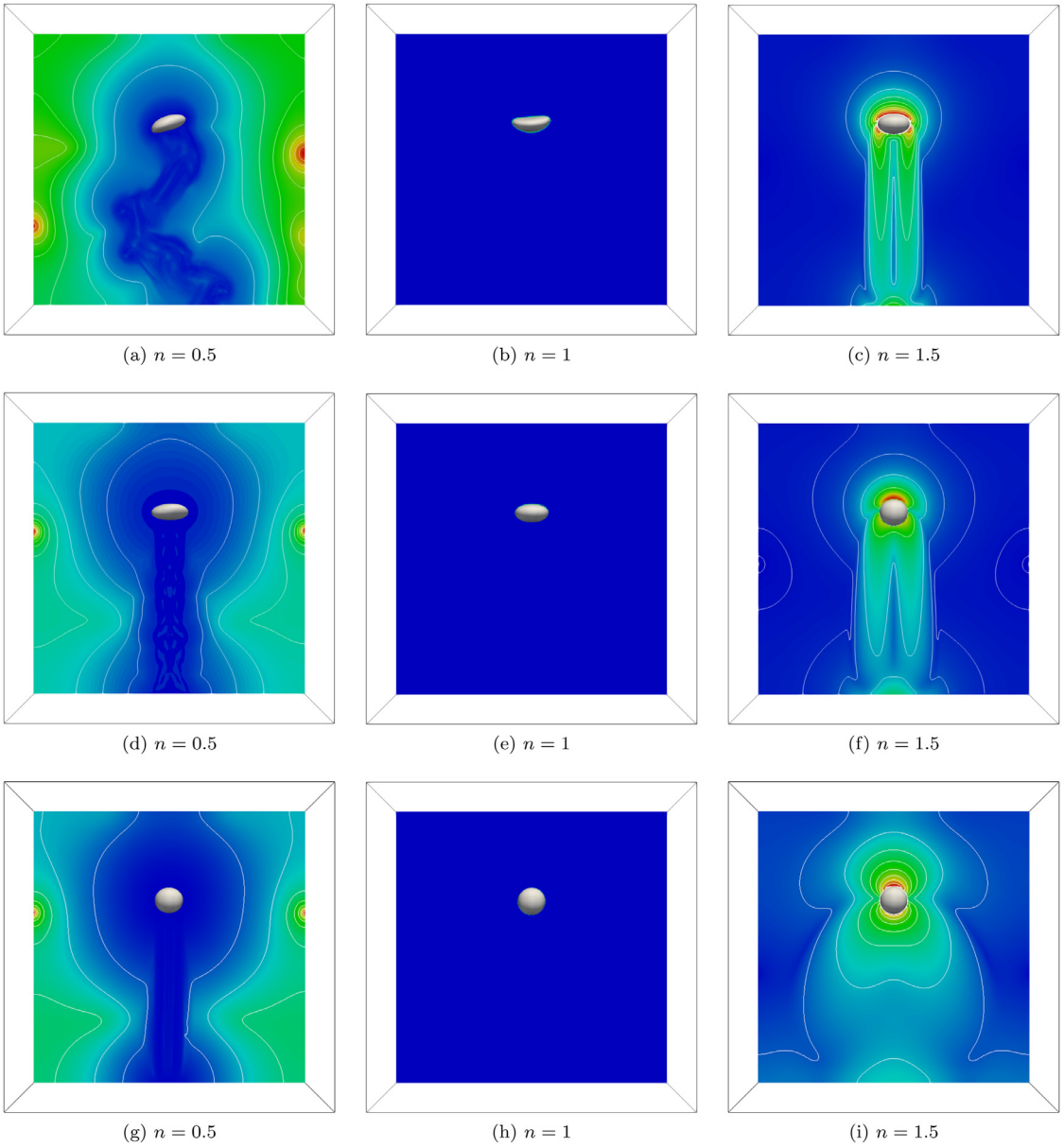

Fig. 4. Apparent viscosity profiles at 1s of simulation time around a (a), (b), and (c) 4 mm; (d), (e), and (f) 2 mm; (g), (h), and (i) 0.5 mm bubble in three different fluids: *left* shear-thinning, *middle* Newtonian and *right* shear-thickening. The colors range from lower (blue) to higher viscosity (red). (For interpretation of the references to color in this figure legend, the reader is referred to the web version of this article.)

Table 4
Physical properties of the air-water system.

Property	Symbol	Value
Gas density	ρ_g	$1.25\,\mathrm{kgm^{-3}}$
Gas viscosity	μ_g	1.8×10^{-5} Pas
Liquid density	ρ_l	$1000\,\mathrm{kgm^{-3}}$
Surface tension	σ	$0.073\,\mathrm{Nm^{-1}}$

Table 5
Overview of the numerical setup.

Setting	Value
Eulerian grid	$200 \times 200 \times 200$
Domain size/bubble diameter	10
Bubble diameter/grid ratio	20
Time step	1×10^{-5} s
Total simulation time	1 s

- a Newtonian region close to the walls (maximum shear)
- a power-law region in between
- a Newtonian region close to the center (no shear)

Since the $\dot{\gamma}$ limits are selected as broad as possible, the two Newtonian regions are reduced to a very small region of the domain, so that it is possible to assume that the power-law model holds in the entire domain.

Table 6
Settings used in the different simulation cases.

Case	d_b [mm]	K [mPas^n]*	Eo[−]	n [-]
1	4.0	1;10;100	2.15	0.5;0.8;1;1.2;1.5
2	0.5		3.35×10^{-2}	
3	2.0		0.54	

* *Different viscosity limits, see* Table 1.

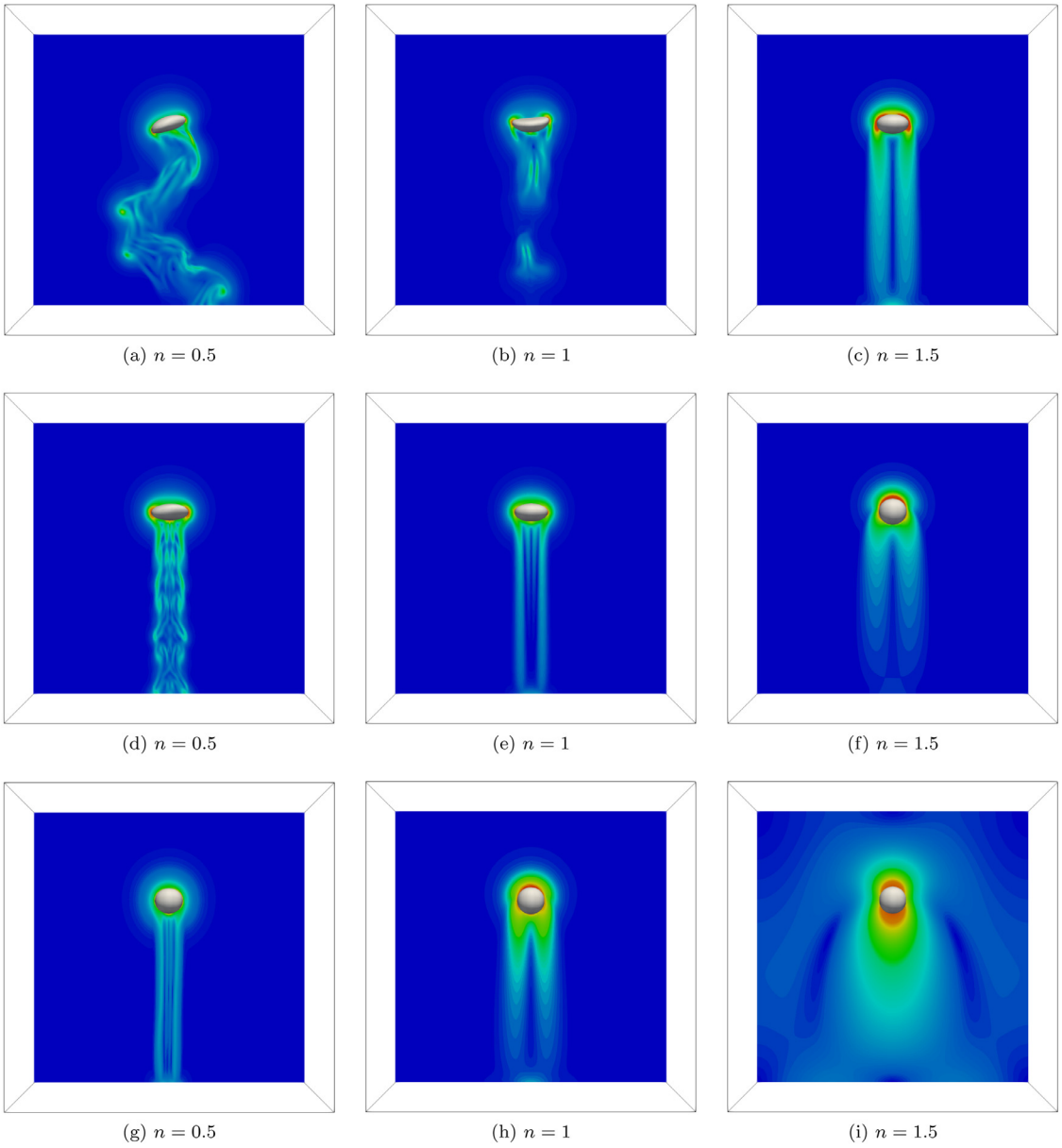

Fig. 5. Profiles of the shear rate ($\dot{\gamma}$) at 1s of simulation time around a (a),(b), and (c) 4 mm; (d),(e), and (f) 2 mm; (g),(h), and(i) 0.5 mm bubble in three different fluids: *left* shear-thinning, *middle* Newtonian and *right* shear-thickening. The colors range from lower (blue) to higher shear rates (red). (For interpretation of the references to color in this figure legend, the reader is referred to the web version of this article.)

The simulations have been carried out with a rectangular domain where the distance between the plates (12 mm) is much smaller than in both other directions (50 cm). In the y-direction (perpendicular to the direction of the flow) a number of 100 grid cells has been used. The two plates have a no slip boundary condition, while for the depth (the z-direction) a free slip boundary is applied. The other simulations parameters are: a time step of 10^{-2} s, an inlet velocity of $u_{in} = 0.01\,\mathrm{ms}^{-1}$, a fluid density of 1000 kg/m^3 and a consistency index $K = 10^{-3}$ Pas^n).

Several flow behaviour indices have been tested, including a fully Newtonian case for completeness. The results of the validation are shown in Fig. 2.

The relative error has been calculated as in Eq. (16) for all the cases, and is given in Table 2.

$$\epsilon_{rel} = \frac{\left\| \mathbf{u}_x - \mathbf{u}_x^{analytical} \right\|_2}{\left\| \mathbf{u}_x^{analytical} \right\|_2} \tag{16}$$

Note that the relative error here is always a positive value, while the relative error in the next sections is calculated without the norm to show the sign of the deviations. The simulation results match very well with the analytical solutions, with a maximal error of only 0.36%, thus confirming the implementation of the viscosity model and the validity of the power-law regime in the whole domain. It is important to mention that the grid used for the actual rising bubble simulations is twice as refined in all directions, in order to accurately capture all dynamic fluctuations in shear rates in the domain, which is one of the main outcomes of the grid dependency study presented below.

3.2. Grid dependency

The dependency of the terminal rise velocity of a bubble on the resolution of both the computational domain and the bubble itself has been studied. In the grid-dependency investigation by Dijkhuizen et al. [1] for bubbles rising in viscous liquids, the minimally required domain-

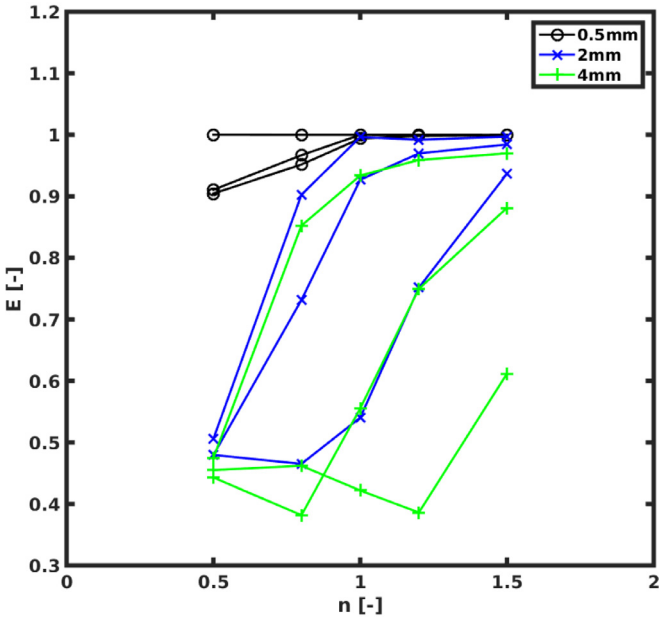

Fig. 6. Bubble aspect ratio E as a function of the exponent n for all the different cases performed.

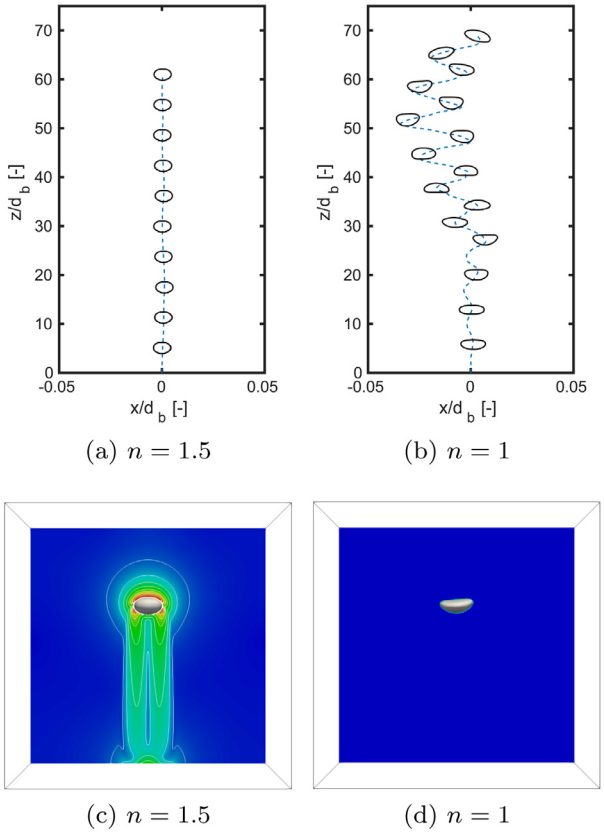

Fig. 7. Comparison of the Newtonian and shear-thickening cases for a 4 mm bubble. (a) and (b), rising patterns. (c) and (d), viscosity profiles. The colors range from lower viscosity (blue) to higher viscosity (red). (For interpretation of the references to color in this figure legend, the reader is referred to the web version of this article.)

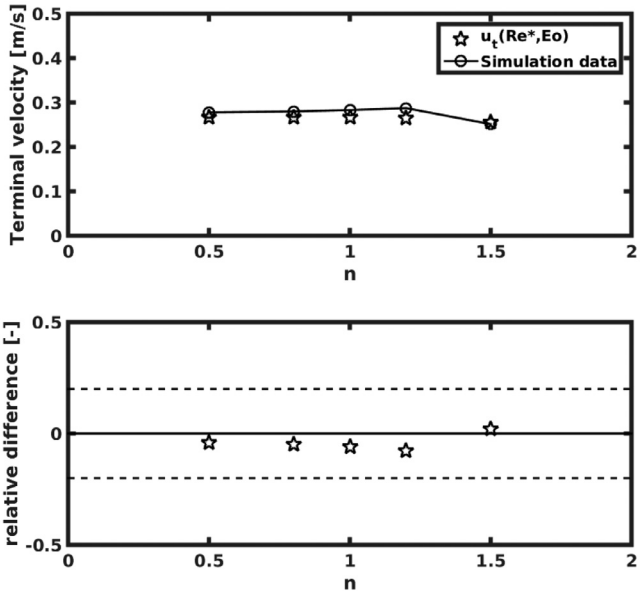

Fig. 8. Terminal velocity of a 4 mm bubble as a function of the non-Newtonian exponent n for a consistency index $K = 10^{-3}$ Pas^n.

to-bubble ratio was determined to be 10, in order to adequately resolve both the bubble motion and the profiles in the domain with sufficient detail; in smaller domain sizes the hydrodynamics is not adequately captured.

To show the effect of the grid resolution, a grid convergence study has been performed using a 4 mm bubble in a Newtonian, a shear-thinning and a shear-thickening liquid with a consistency index $K = 10^{-3}$ Pas^n. The bubble is wobbling in both the Newtonian and shear-thinning liquids and thus indicates the minimum number of grid cells required in a bubble diameter to fully capture the dynamic motion of the gas-liquid interface. For the shear-thickening case, the bubble interface is much less dynamic, as the bubble interface remains nearly or completely spherical while rising, and shows strong similarities to the high-viscosity simulations by Dijkhuizen et al. [1], giving information on the domain-to-bubble ratio.

In such case, both the shear-thinning and the Newtonian bubbles show oscillations in the rise velocity, as a consequence of the wobbling behaviour. In Fig. 3(a), an increasing bubble resolution shows a large difference in the rising velocity profile of the bubble. Indeed, a bubble resolution of at least 20 grid nodes is required to adequately capture the amplitude of the oscillations.

Moreover, from Fig. 3(b) it is visible that the domain size influences the simulation as well. Indeed, the $100 \times 100 \times 100$ grid cells case is not enough to accurately represent the system, especially for more viscous cases where Dijkhuizen et al. [1] showed that a bubble-to-domain ratio of 10 is required. Despite the differences, Table 3 shows that the average terminal velocities are, in all cases, similar with minor deviations between all the different cases, even with a relatively low resolution.

To conclude, to be able to capture both the bubble dynamics and the domain profiles with sufficient detail, a grid of $200 \times 200 \times 200$ with a bubble diameter of 20 grid elements has been selected. A further refinement to the grid has been deemed unnecessary in view of the extensive computational effort already required compared to the expected gain in resolution.

4. Results

With the verified Front-Tracking model, single bubbles rising in various shear-thinning and shear-thickening fluids showing a power-law rheology have been simulated. First, the analysis focuses on the effects

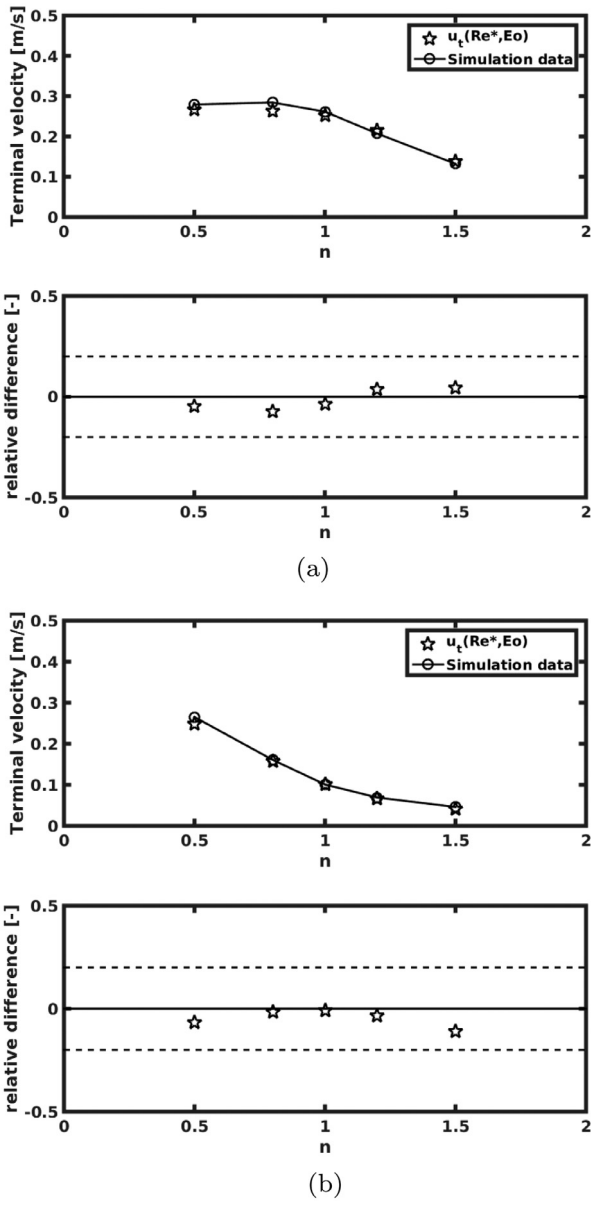

Fig. 9. Terminal velocity of a 4 mm bubble as a function of the non-Newtonian exponent n for different consistency indices: (a) $K = 10^{-2}$ Pas^n and (b) $K = 10^{-1}$ Pas^n.

of the non-Newtonian viscosity profiles on the bubble shape, while the second part will discuss their rise velocity and drag coefficient.

4.1. Numerical setup

As mentioned before, the simulation domain is a cube with $200 \times 200 \times 200$ grid cells. A triangulated mesh of a spherical bubble (with a bubble diameter-to-grid ratio of 20) is placed inside the domain, initialized with zero velocity, with its center at a vertical position of 60% of the domain height. This position allows the bubble wake to be completely resolved, while the velocity field at the top of the domain above the bubble remains quiescent.

With the selected time step of 1×10^{-5} s sufficient temporal resolution is achieved and the simulation is continued for 1 s simulation time, in order to obtain a pseudo-steady state, also for the larger bubbles that are known to oscillate during their rise. An initial transient period of 0.2 s is discarded for the time-averaging to determine the terminal velocity of the bubble and the drag coefficient, as described in more detail in Section 2.5. An overview of the selected numerical settings is provided in Table 5.

The default physical properties are chosen to represent the air-water system for the Newtonian cases (see Table 4), while the apparent viscosity is described with the power-law model given by Eq. (7). Simulations have been performed for different values for the exponent and for different bubble diameters, as detailed in Table 6, while for all the selected bubble diameters three different consistency indices K (1, 10 and 100 times the one of water) have been chosen. For these cases, also the viscosity limits, described in Eq. (7), have been increased by one or two orders of magnitude, accordingly. For all the cases, simulations with $n = 0.5, 0.8, 1, 1.2$ and 1.5 have been performed.

4.2. Apparent viscosity profiles and bubble shape

The non-Newtonian behaviour of the continuous phase has a large influence on the bubble shape, as well as on the bubble behaviour. In Figs. 4 and 5, snapshots of the bubble for the different cases are shown together with the apparent viscosity profiles and shear rate profiles (namely $\dot{\gamma}$). It is possible to immediately recognize the direct correspondence between the magnitude of the shear rate and the apparent viscosity. For instance, Figs. 4(a) and 5(a) show a complementary image of the shear profiles and the apparent viscosity. The bubble is clearly rising in a meandering motion, as noticeable from the wake. In all cases, the front and wake of the bubble are the regions of higher shear, meaning lower or higher viscosity depending on the type of fluid. Interestingly, the 2 mm bubble of Fig. 5(d) is wobbling, as clearly visible from the wake shape, but does not meander as much as the 4 mm bubble.

The bubble aspect ratio for all the different cases is shown in Fig. 6. As expected, in all the shear-thickening cases the bubble shape becomes more spherical as a consequence of the increased viscosity in the fluid immediately surrounding the bubble.

As already mentioned, the bubble trajectory is strongly affected by the non-Newtonian behaviour of the fluid: for the 4 mm case, the Newtonian fluid exhibits a meandering and wobbling bubble, whereas for the shear-thickening non-Newtonian cases the same bubble is rising in a straight line, as shown in Fig. 7. This is similar to a bubble rising in a more viscous fluid. The viscosity is mainly affected at the bubble front (where there is a highly shear-thickening region) and then the liquid passes the bubble forming a higher viscosity tail in the wake. Since the larger bubble rises faster, the viscosity reaches a higher maximum value in front of the bubble, while the viscosity is affected in a larger part of the domain for the smaller 0.5 mm bubble.

When inspecting the shear-thinning cases, it is possible to observe that the bubble sphericity has somewhat decreased (see Fig. 6). The meandering 4 mm bubble maintains this behaviour and this is also visible in the viscosity profile which follows the bubble pattern. In all three shear-thinning cases displayed in Fig. 4, two higher viscosity regions can be observed at the walls (as also observed before by Ohta et al. [16]). Interestingly, unlike the shear-thickening case, the regions with a higher viscosity are located at the walls, while regions of lower viscosity are in front of the bubble and in the wake, which follows the meandering path of the bubble for the 4 mm case. Same as before, the 4 mm bubble rises faster, and therefore the viscosity reaches higher (and lower) values due to larger velocity gradients.

The quantification of these effects on the drag coefficient is discussed in the next section.

4.3. Drag coefficient

From the Front-Tracking simulations, the time-averaged terminal rise velocity (and thus the drag coefficient) of a single rising bubble is directly available as part of the solution. The computed time-averaged terminal rise velocity is compared with the terminal velocity $u_t(\mathrm{Re}^*, \mathrm{Eo})$

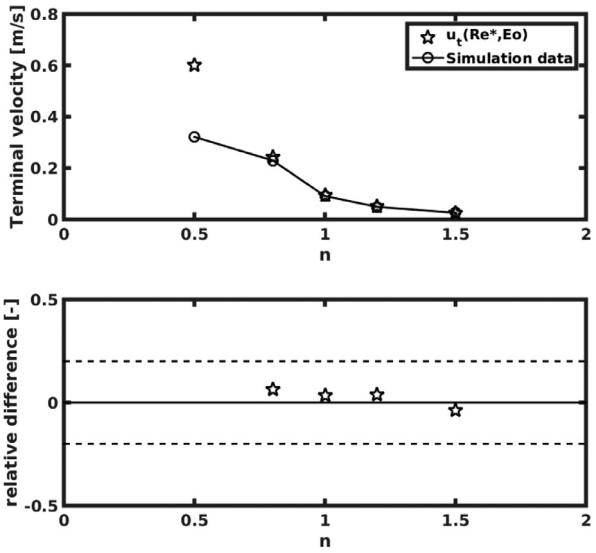

Fig. 10. Terminal velocity of a 0.5 mm bubble as a function of the non-Newtonian exponent n for consistency index $K = 10^{-3}$ Pas^n.

calculated using the drag coefficient detailed in Section 2.5, which is a function of the modified Reynolds number (Re*) given by Eq. (14). In Fig. 8, the terminal velocity of a 4 mm bubble rising in fluids with different non-Newtonian exponents n and consistency index $K = 10^{-3}$ Pas^n is shown. For this case with a relatively large Eo number (Eo = 2.15), the terminal velocity (directly related with the drag coefficient) does not significantly depend on the power-law exponent, because form-drag (viscosity independent) dominates. Only for the case with the highest value for the power-law exponent investigated, viz. $n = 1.5$, the terminal velocity slightly decreases, corresponding to the results of a very shear-thickening liquid. This is due to the higher viscosity, which reduces the Re number slightly and increases the bubble sphericity, causing a small deviation from the drag coefficient expected for a Newtonian fluid, also shown in the figure. Clearly, the correlation is able to predict the terminal rise velocity well and matches the computed Front-Tracking terminal velocity within a 20% deviation margin. When the consistency index K is increased by one or two orders of magnitude (see Fig. 9(a) and (b)), the effect of the highly shear-thickening regime becomes much more pronounced, starting to decrease the terminal velocity of the bubble even more as a consequence of the high viscosity around the bubble itself. The correlation using the modified Reynolds number is still able to predict the bubble terminal velocity considerably well, with deviations within 20%.

For smaller bubbles, the Reynolds number decreases, increasing the contribution of the Reynolds dependent part of the drag on the total drag coefficient. For a 0.5 mm bubble a similar dependency of the terminal velocities on the non-Newtonian exponent is found, as shown in Fig. 10: for exponent values above $n = 1$, the drag coefficient increases drastically, decreasing the terminal velocity of the bubble.

However, despite the similarities in the overall behaviour, there is a large deviation observed between the simulation result and the prediction by the drag correlation based on the modified Reynolds number for the shear-thinning region for small bubbles, where for $n = 0.5$ the error is approximately 87%. This indicates that the correlation is not able to fully describe the drag force in this regime.

First of all, the shape of the bubble is changing from spherical (aspect ratio of 1 for $n = 1$) to slightly ellipsoidal (aspect ratio of 0.9, see Fig. 4(g)). In addition to the shape change, the bubble starts to slightly rise in a meandering motion, as visible in Fig. 12. The cause for the large deviation between the terminal velocity computed with the Front-Tracking model and the velocity predicted by the drag closure is that for

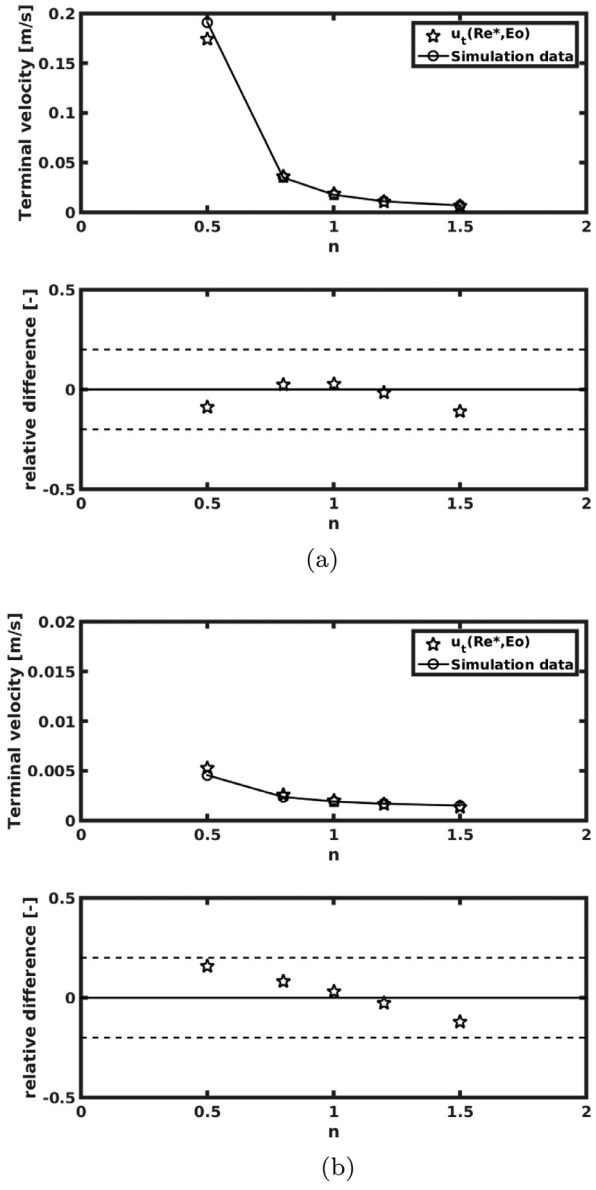

Fig. 11. Terminal velocity of a 0.5 mm bubble as a function of the non-Newtonian exponent n for different consistency indices: (a) $K = 10^{-2}$ Pas^n and (b) $K = 10^{-1}$ Pas^n.

a bubble of this size rising in a Newtonian fluid, the drag on the bubble is dominated by frictional stresses. For the case of a Newtonian fluid, the bubble shape is spherical in this regime and the drag coefficient is dominated by the Reynolds-depending part, which is given by the correlation of Mei et al. [33]. This means that the Eo-dependent part of Eq. (10) is completely negligible, but in the simulation it is not. Indeed, the correlation from Mei et al. [33] does not account for wake dynamics and shape deformations, and the Eo-dependent part (Eq. (12)) was never fitted for bubbles of this size. Because also small bubbles in shear-thinning fluids experience large shape deformations, the application of the closure from Dijkhuizen et al. [1], based on the correlation by Mei et al. [33] for the Reynolds-depending part, will result in a large deviation in the estimation of the terminal velocity. Indeed, for the same bubble diameter rising in more viscous fluids (with a consistency index K higher by one and two order of magnitudes) a much better agreement with the correlation (see Fig. 11) is obtained, where the deviation is again within 20% of deviation. This is consistent with the retained sphericity of the bubble in a more viscous environment. On the other

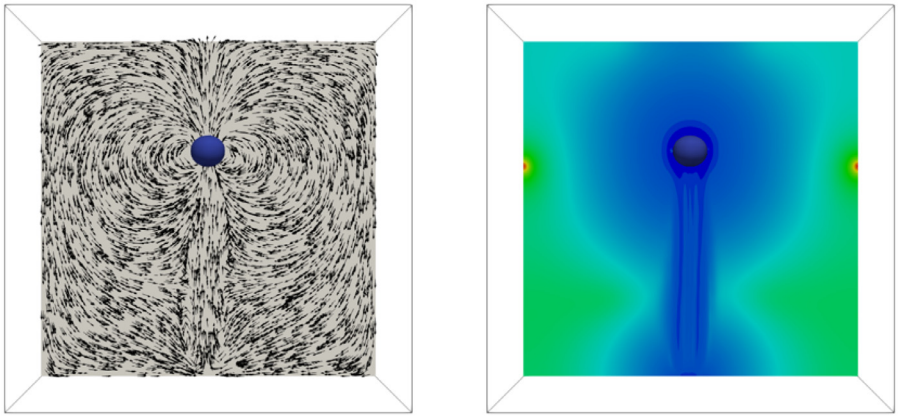

Fig. 12. Highlight of a 0.5 mm bubble rising in a fluids with a non-Newtonian exponent $n = 0.5$ and a consistency index $K = 10^{-3}$ Pas^n. On the left, velocity profile. On the right, viscosity profile.

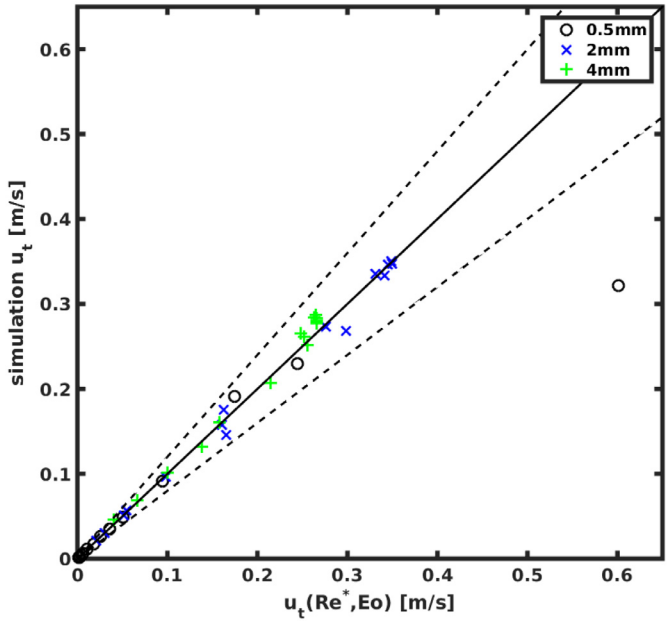

Fig. 13. Parity plot of all simulation cases showing the calculated vs. simulated terminal velocities. The dashed lines represent the ± 20% deviation margin.

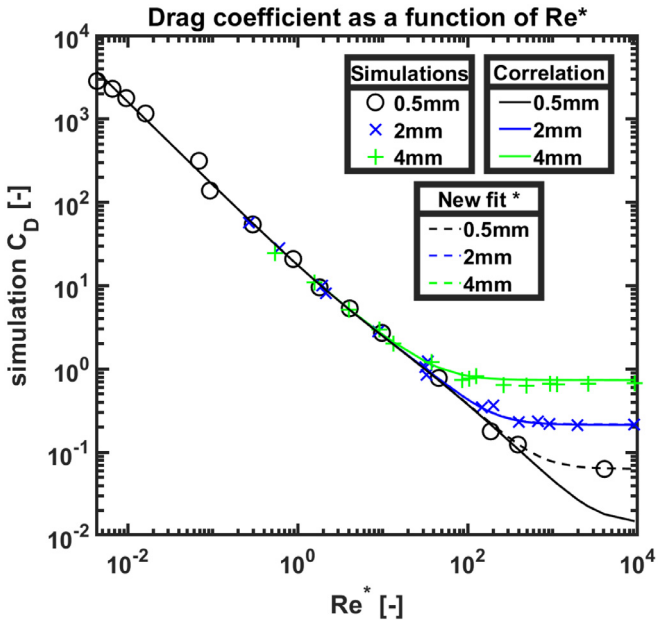

Fig. 14. Drag coefficient as a function of Re* for different bubble sizes. Comparison of simulation results and correlation. * The new fit corresponds to $CD(\mathrm{Eo}) = \frac{4\mathrm{Eo}}{9.5+\mathrm{Eo}} + \frac{1.65\times10^{-3}}{\mathrm{Eo}}$, as suggestion for a better fit.

hand, with a lower exponent $n = 0.2$ for $K = 10^{-2}$ Pas^n, the strong shear-thinning behaviour results again in large deviations in the estimation of the terminal velocity with a deviation of about 74% with an aspect ratio of the bubble of 0.91. As a final remark, the authors want to underline that this specific case describes an extreme type of power-law liquid. Indeed the fluid viscosity reached around the bubble is in the order of the gas viscosity, which would be extremely improbable in nature. More often, shear-thinning fluids present a higher K value, see for instance Venneker et al. [35].

To conclude, a summary of the results is presented in Figs. 13 and in 14, where all the cases described in Table 6 are compared with the terminal velocity and drag coefficient obtained from the correlation of Dijkhuizen et al. [1] using the modified Reynolds number. Here, is noticeable that the case with a bubble diameter of 0.5 mm falls outside the 20% deviation margin, while all the other cases, including the 2 mm bubble, are within 20% of deviation and the majority of occurrences (80% of the cases) lie within 10% of accuracy. The drag coefficient curve shows this as well, where the transition between frictional (Eq. (11)) and form-drag (Eq. (12)) is visible. This is captured very well for the higher Eo number bubbles (i.e. 2 mm and 4 mm), while the transition is not captured well for the 0.5 mm bubble with $n = 0.5$ and $K = 10^{-3}$ Pas^n, as previously discussed. The Eotvos-dependent part of the drag correlation, given in Eq. (12), can be easily adjusted to account for this case, for instance by adding 1.65×10^{-3}/Eo. This will result in a better fit for the transition while marginally affecting higher Eo cases, as shown in Fig. 14. The authors would like to stress to the reader that this is merely a suggestion on how to improve the fitting to include the missing point, because for a proper correction of the drag correlation many more points at different Eo numbers should be included.

5. Conclusions

With a simulation study using a Front-Tracking model, it is shown that non-Newtonian fluids drastically alter the bubble shape as a consequence of the developed viscosity profiles. Especially, large non-spherical bubbles become more spherical in shear-thickening fluids, while the opposite is true for small spherical bubbles in shear-thinning fluids. The drag relation proposed by Dijkhuizen et al. [1], and hereby adapted to use the modified Reynolds number (Re*), is able to predict the drag coefficient and hence the terminal velocity for moderately non-Newtonian fluids (e.g. $0.5 \leq n \leq 1.5$) within 20% accuracy in most cases,

excluding the case for very small bubbles rising in a strongly shear-thinning fluid with very low viscosity, viz. $d_b = 0.5\,\text{mm}$, $K = 10^{-3}\,\text{Pas}^n$ and $n = 0.5$. In this case, the bubble aspect ratio differs strongly from unity and the bubble starts meandering. This behaviour is not accounted for in the drag correlation, as the Newtonian bubble is perfectly spherical and wake dynamics do not play a role. The rise velocity of the same bubble in more viscous fluids with a higher consistency index K do retain their sphericity and do not meander, and the rise velocity is well predicted by the correlation within the 20% deviation margin.

Finally, this work should be further extended to investigate more complex types of fluids, including visco-elasticity and memory effects, and to include swarm effects, ultimately giving the possibility to develop a complete drag closure for unresolved models for all types of fluids.

Declaration of Competing Interest

The authors declare that they have no known competing financial interests or personal relationships that could have appeared to influence the work reported in this paper.

Acknowledgments

This work is part of an Industrial Partnership Programme of the Foundation for Fundamental Research on Matter (FOM) which is part of the Dutch Research Council (NWO). This Industrial Partnership Programme is co-financed by Nouryon Chemicals International B.V., DSM Innovation Center B.V., Sabic Global Technologies B.V., Shell Global Solutions B.V., and Tata Steel Nederland Technology B.V.

References

[1] W. Dijkhuizen, I. Roghair, M. Van Sint Annaland, J.A.M. Kuipers, DNS of gas bubbles behaviour using an improved 3D front tracking model–Drag force on isolated bubbles and comparison with experiments, Chem. Eng. Sci. 65 (4) (2010) 1415–1426.
[2] W.A. Al-Masry, Effect of scale-up on average shear rates for aerated non-Newtonian liquids in external loop airlift reactors., Biotechnol. Bioeng. 62 (4) (1999) 494–498.
[3] H.Z. Li, Bubbles in non-Newtonian fluids: formation, interactions and coalescence, Chem. Eng. Sci. 54 (13-14) (1999) 2247–2254.
[4] R. Darby, R.P. Chhabra, Chemical Engineering Fluid Mechanics, third ed., CRC Press, 2016.
[5] N.G. Deen, M. van Sint Annaland, J.A.M. Kuipers, Multi-scale modeling of dispersed gas-liquid two-phase flow, Chem. Eng. Sci. 59 (8-9) (2004) 1853–1861.
[6] M. Van Sint Annaland, N.G. Deen, J.A.M. Kuipers, Multi-Level Modeling of Dispersed Gas-Liquid Two-Phase Flows, Heat and Mass Transfer, Springer, Berlin, 2003.
[7] Y.M. Lau, I. Roghair, N.G. Deen, M. van Sint Annaland, J.A.M. Kuipers, Numerical investigation of the drag closure for bubbles in bubble swarms, Chem. Eng. Sci. 66 (14) (2011) 3309–3316.
[8] I. Roghair, Y.M. Lau, N.G. Deen, H.M. Slagter, M.W. Baltussen, M. Van Sint Annaland, J.A.M. Kuipers, On the drag force of bubbles in bubble swarms at intermediate and high Reynolds numbers, Chem. Eng. Sci. 66 (14) (2011) 3204–3211.
[9] I. Roghair, M. Van Sint Annaland, J.A.M. Kuipers, Drag force and clustering in bubble swarms, AIChE J. 59 (5) (2013) 1791–1800.
[10] B. Wu, Cfd simulation of gas and non-newtonian fluid two-phase flow in anaerobic digesters, Water Res. 44 (13) (2010) 3861–3874.
[11] X. Frank, H.Z. Li, Complex flow around a bubble rising in a non-newtonian fluid, Phys. Rev. E 71 (2005) 036309.
[12] J. Liu, C. Zhu, T. Fu, Y. Ma, H. Li, Numerical simulation of the interactions between three equal-interval parallel bubbles rising in non-newtonian fluids, Chem. Eng. Sci. 93 (2013) 55–66.
[13] S. Radl, G. Tryggvason, J.G. Khinast, Flow and mass transfer of fully resolved bubbles in non-Newtonian fluids, AIChE J. 53 (7) (2007) 1861–1878.
[14] L. Zhang, C. Yang, Z.-S. Mao, Numerical simulation of a bubble rising in shear-thinning fluids, J. Non-Newtonian Fluid Mech. 165 (11-12) (2010) 555–567.
[15] D. Rodrigue, A simple correlation for gas bubbles rising in power-law fluids, Canad. J. Chem. Eng. 80 (2) (2002) 289–292.
[16] M. Ohta, Y. Yoshida, M. Sussman, A computational study of the dynamic motion of a bubble rising in Carreau model fluids, Fluid Dyn. Res. 42 (2) (2010) 025501.
[17] M. Ohta, S. Kimura, T. Furukawa, Y. Yoshida, M. Sussman, Numerical simulations of a bubble rising through a shear-thickening fluid, J. Chem. Eng. Japan 45 (9) (2012) 713–720.
[18] A.R. Premlata, M.K. Tripathi, B. Karri, K.C. Sahu, Numerical and experimental investigations of an air bubble rising in a carreau-yasuda shear-thinning liquid, Phys. Fluids 29 (3) (2017) 033103.
[19] A.R. Premlata, M.K. Tripathi, B. Karri, K.C. Sahu, Dynamics of an air bubble rising in a non-newtonian liquid in the axisymmetric regime, J. Non-Newtonian Fluid Mech. 239 (2017) 53–61.
[20] K.C. Sahu, A review on rising bubble dynamics in viscosity-stratified fluids, Sādhanā 42 (4) (2017) 575–583, doi:10.1007/s12046-017-0634-8.
[21] A.R. Premlata, M.K. Tripathi, K.C. Sahu, Dynamics of rising bubble inside a viscosity-stratified medium, Phys. Fluids 27 (7) (2015) 072105, doi:10.1063/1.4927521.
[22] M.K. Tripathi, K.C. Sahu, G. Karapetsas, O.K. Matar, Bubble rise dynamics in a viscoplastic material, J. Non-Newtonian Fluid Mech. 222 (2015) 217–226, doi:10.1016/j.jnnfm.2014.12.003.
[23] J. Tsamopoulos, Y. Dimakopoulos, N. Chatzidai, G. Karapetsas, M. Pavlidis, Steady bubble rise and deformation in newtonian and viscoplastic fluids and conditions for bubble entrapment, J. Fluid Mech. 601 (2008) 123–164, doi:10.1017/S0022112008000517.
[24] R. Chhabra, Motion of spheres in power law (viscoinelastic) fluids at intermediate reynolds numbers: a unified approach, Chem. Eng. Process.: Process Intensif. 28 (2) (1990) 89–94, doi:10.1016/0255-2701(90)80004-O.
[25] M.W. Baltussen, L.J.H. Seelen, J.A.M. Kuipers, N.G. Deen, Direct numerical simulations of gas-liquid-solid three phase flows, Chem. Eng. Sci. 100 (2013) 293–299.
[26] M.W. Baltussen, J.A.M. Kuipers, N.G. Deen, Direct numerical simulation of effective drag in dense gas-liquid-solid three-phase flows, Chem. Eng. Sci. 158 (2017) 561–568.
[27] I. Roghair, M. Van Sint Annaland, J.A.M. Kuipers, An enhanced front tracking method featuring volume conservative remeshing and mass transfer, Progress Appl. CFD (2015) 59–71.
[28] I. Roghair, M. Van Sint Annaland, J.A.M. Kuipers, An improved front-tracking technique for the simulation of mass transfer in dense bubbly flows, Chem. Eng. Sci. 152 (2016) 351–369.
[29] W. Dijkhuizen, I. Roghair, M. Van Sint Annaland, J.A.M. Kuipers, DNS of gas bubbles behaviour using an improved 3D front tracking model–Model development, Chem. Eng. Sci. 65 (4) (2010) 1427–1437.
[30] R.B. Bird, W.E. Stewart, E.N. Lightfoot, Transport Phenomena, revised 2nd ed., John Wiley & Sons, New York, 2007.
[31] S. Gabbanelli, G. Drazer, J. Koplik, Lattice Boltzmann method for non-Newtonian (power-law) fluids, Phys. Rev. E – Stat. Nonlinear Soft Matter Phys. 72 (4) (2005) 046312.
[32] A. Prosperetti, Navier-Stokes numerical algorithms for free-surface flow computations: an overview, Drop-Surf. Interact. 456 (2002) 237–257.
[33] R. Mei, J.F. Klausner, C.J. Lawrence, A note on the history force on a spherical bubble at finite Reynolds number, Phys. Fluids 6 (1) (1994) 418–420.
[34] R.P. Chhabra, Bubbles, Drops, and Particles in Non-Newtonian Fluids, Second Edition, Chemical Industries, CRC Press, 2006.
[35] B.C.H. Venneker, J.J. Derksen, H.E.A. van den Akker, Turbulent flow of shear-thinning liquids in stirred tanks–the effects of Reynolds number and flow index, Chem. Eng. Res. Des. 88 (7) (2010) 827–843.